Inhomogeneous transient uniaxial extensional rheometry

Jonathan P. Rothstein[a)] and Gareth H. McKinley

Department of Mechanical Engineering, Massachusetts Institute of Technology, Cambridge, Massachusetts 02139

(Received 20 May 2002; final revision received 28 August 2002)

Synopsis

A filament stretching rheometer is used to probe the development of coil-stretch hysteresis in transient nonhomogeneous uniaxial elongation of a dilute polymer solution. Laser-Doppler velocimetry measurements are used to measure the steady centerline velocity profile in an elastic test fluid as it flows towards the throat of a 4:1:4 axisymmetric contraction/expansion over a range of Deborah numbers. The corresponding time-varying extension rate experienced by a fluid element as it flows into the contraction is then downloaded to a filament stretching rheometer in order to impose an identical inhomogeneous stretch history. Simultaneous optoelectronic measurements of the flow induced birefringence and mechanical measurements of the total tensile force in the filament allow independent determination of the evolution in the conformational anisotropy and stress. A pronounced stress-conformation hysteresis is observed with the relationship between the polymeric tensile stress and the average anisotropy in the polymer coil conformation evolving differently during the imposed extension and subsequent relaxation. An energy dissipation per unit volume can be calculated from the area enclosed by the stress-conformation hysteresis loop. The critical Deborah number for the onset of hysteresis and the scaling of the energy dissipation with an increase in deformation rate are found to correlate closely with the development of the additional drop in pressure that is measured macroscopically during viscoelastic flow through the contraction/expansion. These macroscopic and microscopic measurements both support the existence of an additional dissipative contribution to the polymer stress which must be resolved by constitutive models in order to accurately simulate complex flows of elastic polymer solutions. [DOI: 10.1122/1.1516788]

I. INTRODUCTION

The dynamical response of polymeric fluids in extensional or ''strong'' flows is markedly different than in simple shear, and for this reason, extensional rheology is a topic of continued interest and importance to the polymer community. For dilute polymer solutions, recent developments in both experimental techniques and computational algorithms have led to new insights into the rheological response of these fluids [see, for example, Nguyen and Kausch (1999); McKinley and Sridhar (2002)]. These studies have revealed that even in a simple homogeneous extensional deformation, the evolution in the polymeric microstructure and the associated elastic stress in the solution can be more complex than first expected. Such molecular complexities are also important in flows with mixed kinematics that are encountered in industrial processing operations such as film coating and fiber spinning. If large-scale numerical simulations are to be useful as optimization or

[a)]Author to whom all correspondence should be addressed; electronic mail: rothstein@ecs.umass.edu

design tools for such processes, then it is essential that the constitutive models can accurately predict the evolution in both the microstructure and the viscoelastic stresses in the fluid as well as their impact on global measures such as the drop in pressure or drag or spinline tension. In the present work, we focus on investigating the response of a model dilute polymer solution in a prototypical complex geometry: the flow through an axisymmetric contraction/expansion.

Contraction flows expose fluid elements to rapid transient extensional deformation and it is well known that the response of a viscoelastic fluid can be very complex in such geometries [Boger (1987)]. Macroscopic measurements of the extra drop in pressure in this geometry have been considered extensively as a device for characterizing the extensional viscosity of non-Newtonian fluids [see Cogswell (1972); Binding and Walters (1988) for more details]. However, the flow in a contraction-expansion geometry is a complex flow with wall regions of strong shearing deformation encapsulating the extensional deformation near the centerline. Detailed numerical studies show that it can thus be extremely difficult to clearly associate the pressure-drop/flow-rate data with local deformation of fluid elements [Rajagopalan (2000)]. It is thus necessary to combine macroscopic measurements with more localized probes of the fluid deformation such as light scattering or flow-induced birefringence.

Flow-induced birefringence measurements of dilute and semidilute polymer solutions that undergo transient uniaxial elongation in a filament stretching device were first reported by Doyle *et al.* (1998). Experimental measurements coupled with Brownian dynamic simulations revealed the existence of a ''stress-conformation'' hysteresis. Doyle *et al.* (1998) found that in a strong stretching flow the average configuration and resulting stress in a polymer chain evolved along different paths during stretching and relaxation. This hysteresis was shown to arise from nonequilibrium coupling between the macroscopic flow field and the internal degrees of freedom of the fluid microstructure. These hysteresis loops are predicted by Brownian dynamics computations using ensembles of bead-rod chains [Doyle *et al.* (1998)] and non-Hookean dumbbells [Sizaire *et al.* (1999)] but cannot be captured by simpler closed-form constitutive models that do not resolve the internal nonequilibrium configurations of the polymer chains. Detailed experimental studies [Smith and Chu (1998)] and numerical analysis [Agarwal (2000); Li *et al.* (2000); Ghosh *et al.* (2002)] of large numbers of molecular conformations show that it is the distribution of initial configurational states that leads to the ''molecular individualism'' on the microscopic scale and the resulting hysteresis in ensemble averaged quantities such as the total flow-induced birefringence and polymeric stress.

It has been conjectured that the failure to resolve such features of transient elongational behavior of polymer solutions may explain the discrepancy between experimental measurements and computations of macroscopic quantities such as the extra drop in pressure in the contraction-expansion geometry and the enhanced drag coefficient of a sphere sedimenting through an elastic fluid [Rothstein and McKinley (2001)]. Preliminary calculations using a new constitutive model that captures the general characteristics of this hysteresis support this suggestion [Joo *et al.* (2001)]. To definitively address this question, it is desirable to make simultaneous measurements of the birefringence and stress experienced by fluid elements as they flow along extensionally dominated streamlines such as the centerline of an axisymmetric contraction/expansion.

There are at least two significant difficulties in performing such measurements: (i) most implementations of flow-induced birefringence are an integrative or line-of-sight technique and thus measurements in an axisymmetric geometry are convolutions of the strong shearing deformations near the walls and the transient extension near the centerline; (ii) furthermore, even if the local birefringence could be obtained, it is then neces-

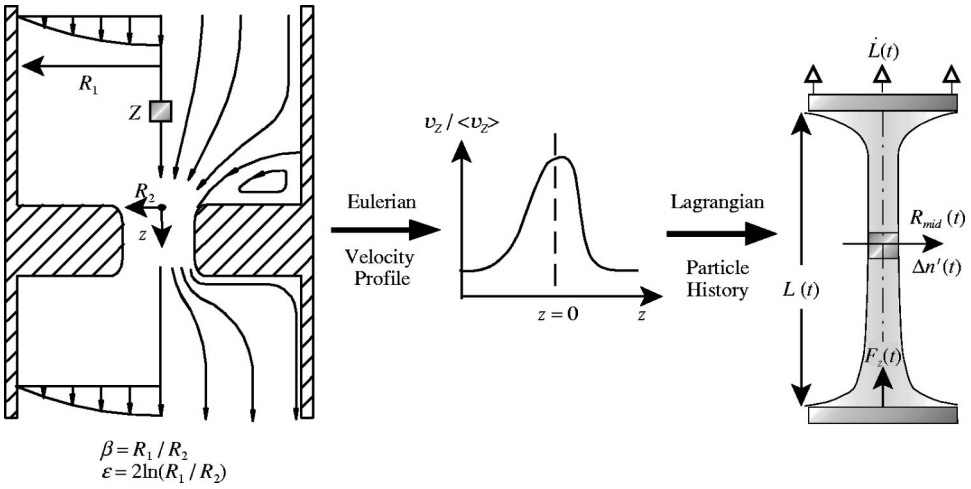

FIG. 1. Outline of the conversion of the velocity profiles experienced by a fluid element moving along the centerline upstream of a 4:1:4 axisymmetric contraction/expansion into a inhomogeneous uniaxial elongational profile imposed by a filament stretching rheometer.

sary to invoke the stress-optical rule in order to compute the stress since no independent pointwise measure of stress is available, only integrated quantities such as the total drop in pressure or net drag force across the geometry.

In a planar geometry the first difficulty can be alleviated and pointwise measurements of the local velocity field can be used to compute the deformation rate experienced by a fluid element as it flows through the contraction. If the stress-optical rule holds, as expected for semidilute or concentrated entangled fluids up to high stresses or deformation rates [Venerus *et al.* (1999); Rothstein and McKinley (2002)], it is then possible to compare measurements of the birefringence with predictions of different constitutive models in transient planar elongation [Quinzani *et al.* (1995)]. The analysis is more difficult in axisymmetric geometries, because the signals measured are an integrated retardance and total orientation angle [Li *et al.* (1998)]; however, these integrated quantities can be compared with equivalent values obtained from full numerical simulations using an appropriate constitutive model [Li *et al.* (1998); Nguyen *et al.* (1999)]. A detailed comparison of the experimental results with numerical computations is impeded, however, by the expected failure of the stress-optical rule (due to stress-conformation hysteresis) on the microscale, and the corresponding failure of numerical computations to capture the macroscopic pressure-drop/flow-rate curves measured experimentally [Szabo *et al.* (1997); Rothstein and McKinley (2000)].

Given this difficulty, we have pursued a different approach which effectively isolates the extensional region of the flow field. Our approach is summarized in Fig. 1. A noninvasive LDV system is used to measure the steady Eulerian velocity field (and its evolution with an increase in flow rate or Deborah number) along the centerline of a 4:1:4 axisymmetric contraction/expansion. These measurements are then used to compute the Lagrangian deformation history experienced by fluid elements as they flow through the contraction/expansion. The corresponding strain rate history is inhomogeneous in time—with very low extension rates upstream and rapid deformation close to the contraction plane. Recent Brownian dynamics simulations [Hernandez Cifre and de la Torre (1998)] in a model inhomogeneous extensional flow with a time-varying extension rate indicated that molecular individualism and conformational hysteresis still arise in such inhomoge-

neous flows when the extension rate rises above the critical value for the coil-stretch transition that is determined independently in a homogeneous extensional flow.

The strain-rate history computed from the kinematic measurements in the contraction-expansion geometry is subsequently downloaded to the motion control system of a filament stretching rheometer. In a filament stretching test, time-resolved measurements of the evolution in diameter at the axial midplane of the device can be used to confirm the deformation rate experienced by the fluid element at this location, and independent optical and mechanical measurements of the birefringence and total extensional stress in the fluid can be simultaneously obtained. Thus the main focus of the research presented in this article is to use these measurements to determine the stress-conformation response of the dilute polymer solution in inhomogeneous transient extensional flows and its correlation (if any) to macroscopic measurements such as the pressure-drop/flow-rate relationship in the original flow geometry.

The outline of this article is as follows. In Sec. II, we briefly describe the implementation of the birefringence and filament stretching techniques, the rheology of the test fluid and the particular form of the extensional deformation history we use. In Sec. III A, we first confirm the presence of stress-optical hysteresis in homogeneous extensional flow and in Sec. III B we then present results for the inhomogeneous case as the characteristic extension rate (or Deborah number) of the flow is progressively increased. Finally, we compare these measurements with corresponding macroscopic mechanical measurements of the extra drop in pressure measured in the actual contraction-expansion geometry.

II. EXPERIMENTAL TECHNIQUE

A. Filament stretching rheometer

Many research groups around the world have developed filament stretching rheometers of various designs and operating spaces [McKinley and Sridhar (2002)]. In a recent paper, Anna *et al.* (2001) reported the results of an interlaboratory comparison of filament stretching rheometers in which several different instruments were used to study three dilute polystyrene-based elastic fluids. Excellent agreement was achieved among different instruments. Filament stretching rheometry is now sufficiently well developed that it can provide quantitative experimental data for the transient extensional stress growth of polymeric fluids.

The filament stretching rheometer (FiSER) used to make the measurements presented in this study follows closely the successful design of Anna (2000). In this device, an initially cylindrical filament of fluid is stretched between two circular endplates. The linear stage consists of two brushless linear dc motors which are used to impose a known velocity profile on the two platens. The upper motor controls the velocity profile of the top endplate while the lower motor, traveling at half the velocity of the upper motor, ensures that an array of measurement devices is kept at the midpoint of the elongating fluid filament. The motion control system is manufactured entirely by Compumotor (6250) and has a resolution of 0.02 cm in its vertical positioning, a maximum travel of 100 cm, a maximum velocity of 100 cm/s and a maximum acceleration of 6000 cm/s^2. The imposed velocity profiles and the data acquisition are controlled entirely through LABVIEW. A load cell (Futek L2338) is mechanically isolated from the linear stage and mounted to the lower endplate. The force transducer has a maximum measurable load of 10 grams with a resolution of ± 5 mg. The midpoint diameter is measured with a laser micrometer with a resolution of ± 20 μm (Omron Z4LA). The calibrated resolution of the

laser micrometer is ± 20 μm. A flow-induced birefringence (FIB) measurement optical train is also mounted on the lower platen and is discussed in more detail in Sec. II B.

A representative sketch of a typical fluid filament within the filament stretching rheometer is shown in Fig. 1. The time evolving length of the filament is denoted $L(t)$ while $R_{\text{mid}}(t)$ is the midpoint radius of the filament, $F_z(t)$ is the force exerted by the filament on the endplate, $\dot{L}(t)$ is the velocity of the endplate, and L_0 and R_0 are the initial length and radius of the fluid filament, respectively. In an ideal homogeneous uniaxial extensional flow a cylindrical fluid sample is separated exponentially in time [Bird *et al.* (1987a)]. However, in practice the elongation is nonideal and the center regions of the fluid filament experience a time-dependent effective stretch rate, $\dot{\epsilon}_{\text{eff}}(t)$. This effective deformation rate can be determined directly from the filament radius,

$$\dot{\varepsilon}_{\text{eff}}(t) = -\frac{2}{R_{\text{mid}}(t)}\frac{dR_{\text{mid}}(t)}{dt}. \tag{1}$$

The total deformation of this fluid element is characterized by the Hencky strain measure which is the integral of the effective strain rate over all time,

$$\varepsilon_{\text{eff}} = \int_0^t \dot{\varepsilon}_{\text{eff}}(t')dt' = -2\ln(R_{\text{mid}}/R_0). \tag{2}$$

If a constant stretch rate is applied to the endplates, this test is classified as a type II experiment [Kolte *et al.* (1997)]. If the test is designed in such a way that the effective strain rate is constant, $\dot{\varepsilon}_{\text{eff}} = \dot{\varepsilon}_0$, then the test is classified as a type III experiment. To accurately determine the desired material properties of the elastic fluid, type III experiments must be performed. An effective technique for reproducibly generating type III tests from type II ''master curves'' has recently been developed [Anna *et al.* (1999); Orr and Sridhar (1999)] and has been employed in all the experiments presented in this article.

Filament stretching rheometers have historically been used to measure the transient extensional viscosity of polymeric fluids in homogeneous uniaxial extension at a constant deformation rate ($\dot{\varepsilon}_0$). The extensional viscosity function is defined by

$$\eta_E^+(\dot{\varepsilon}_0,t) = \frac{\langle \tau_{zz}-\tau_{rr}\rangle}{\dot{\varepsilon}_0}, \tag{3}$$

where $\langle \tau_{zz}-\tau_{rr}\rangle$ is the principal tensile stress difference generated within the filament. In a detailed force balance of the filament stretching rheometer, Szabo *et al.* [Szabo *et al.* (1997)] showed that the difference in tensile stress generated within the filament can be calculated from the total force measured by the load cell, F_z, if the weight of the fluid, the surface tension and the inertia of the fluid are taken into account. For the case of a stationary lower plate and midplane acceleration of $\ddot{z}_0 = \ddot{L}_z/2$, the force balance becomes

$$\langle \tau_{zz}-\tau_{rr}\rangle = \frac{F_z}{\pi R_{\text{mid}}^2} + \frac{1}{2}\frac{\rho g(\pi L_0 R_0^2)}{\pi R_{\text{mid}}^2} - \frac{\sigma}{R_{\text{mid}}} + \frac{1}{2}\frac{\rho(\pi L_0 R_0^2)\ddot{L}_z}{\pi R_{\text{mid}}^2}, \tag{4}$$

where σ is the surface tension of the fluid, ρ is the density of the fluid and $\ddot{L}_z$ is the acceleration of the upper endplate. The last term in Eq. (4) is due to fluid inertia and is, in practice, negligibly small for the test fluids considered in the present work. In homogeneous uniaxial extension a dimensionless extensional viscosity or the Trouton ratio

$\mathrm{Tr}^+ = \eta_E^+/\eta_0$ is often reported. However, if the extension rate is not constant, then the Trouton ratio may not be the best dimensionless form with which to report the evolution of the difference in tensile stress. If we look at the form of the polymeric stress for the ith mode of a Rouse chain,

$$\tau_{p,i} = -n_p k_B T(\mathbf{A}_i - \mathbf{I}), \tag{5}$$

where $\mathbf{A}_i$ is the dimensionless polymer conformation tensor for the ith Rouse mode, then an alternative way to nondimensionalize the polymeric stress is to use the elastic modulus, $n_p k_B T$, where n_p is the number density of polymer chains in the solution and k_B is the Boltzmann constant. This choice of stress scale is also useful in presenting flow-induced birefringence measurements, which we discuss below.

B. Flow-induced birefringence

The molecular polarizability and hence the macroscopic refractive index of a typical linear homopolymer chain is different in the direction parallel to and normal to the chain backbone [Fuller (1995)]. Flow-induced birefringence utilizes this refractive index mismatch to probe the microscopic deformation of polymer chains. Optical birefringence measurements are noninvasive and extremely sensitive to small changes in the local orientation and deformation of polymer chains. By passing light of known polarization state and frequency through the polymeric fluid sample and measuring the resulting change in polarization state, flow-induced birefringence can be used to determine the local anisotropy in the conformation of the polymer chains that undergo both steady and time-varying deformation [Fuller (1995)]. For a flexible polymer chain, the resulting expression for the birefringence can be written in the form

$$\frac{\Delta n'}{C} = n_p k_B T \Delta A, \tag{6}$$

where $\Delta n'$ is the measured birefringence, C is the stress-optical coefficient and $\Delta A = A_{11} - A_{22}$ is a measure of the anisotropy in the average conformation of the polymer chain. The polymer conformation is characterized by the dimensionless second moment tensor, $\mathbf{A} = \langle \mathbf{QQ} \rangle / Q_{\mathrm{eq}}^2$, where $\mathbf{Q}$ is the end-to-end vector of the polymer chain and Q_{eq}^2 is the equilibrium size of the coiled chain. To be consistent with the values in the literature for polystyrene in an aromatic solvent, a stress-optical coefficient value of $C = -5.0 \times 10^{-9}$ Pa^{-1} will be used in all of our FIB calculations [Doyle *et al.* (1998); Venerus *et al.* (1999)].

The optical path for the polarization modulated flow birefringence system employed in this research is shown in Fig. 2(a) and is similar in design to the system pioneered by Frattini and Fuller (1984). The kernel of the current birefringence system was developed jointly with NASA's Glenn Research Center for use in filament stretching experiments in microgravity. The rigors of unmanned sounding rocket experimentation require that the system be robust, compact and sensitive. The system is light, insensitive to mechanical vibration and can be successfully mounted to the lower moving platen of the filament stretching rheometer. The operation and calibration of this system with a dual-crystal electro-optical modulator have been presented previously by Mackey and co-workers (1999). The polarized laser light is generated by a 4.5 mW, 635 nm laser diode (Thorlabs CPS43AP05ME). The light is first passed through a linear polarizer (New Focus 5524) oriented 0° from the vertical axis of the filament stretching rheometer. The polarized light is then sent through a dual-crystal electro-optical modulator oscillating at 44 kHz and

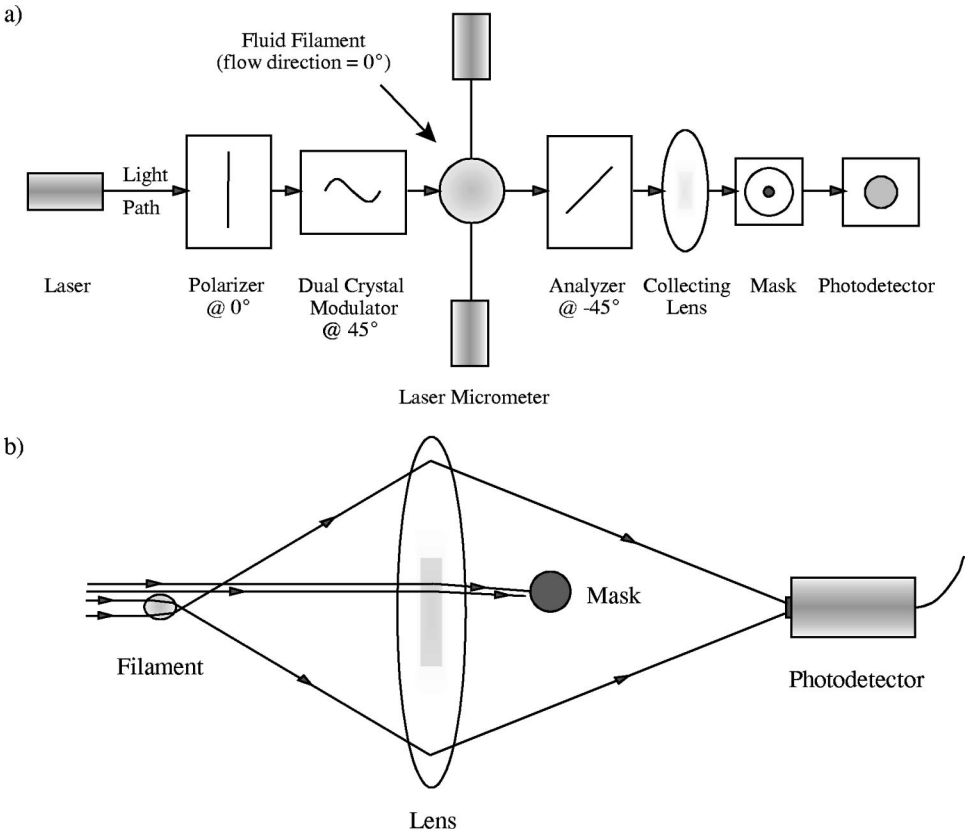

FIG. 2. Schematic diagram in the (x, y) plane of (a) the flow-induced birefringence optical train and (b) the masking technique.

oriented at 45°. After passing through the filament, the light reaches a second linear polarizer, known as the analyzer, which is oriented at $-45°$. Finally, the light passes through a biconvex collecting lens (Newport KBX39) and a mask before impinging on a photodetector (Thorlabs PDA55).

There are several major difficulties associated with successfully taking optical measurements of a thinning fluid column in a filament stretching rheometer. The radial curvature of the filament acts like a cylindrical lens, fanning the laser light and dramatically reducing the intensity of the light reaching the photodetector. As the filament shrinks, the magnitude of the light spreading will increase. Depending on the axial strain imposed, the filament may become smaller than the cross section of the incoming laser beam and allow laser light which has passed around the filament to reach the photodetector. To correct both of these problems, a lens and a mask were arranged as shown in Fig. 2(b). A similar idea was presented and analyzed by Talbott (1978). The lens is placed such that the diverging light exiting the filament is refocused onto the photodetector. The light that passes around the filament is not spread and is blocked by the mask which is composed of a black cylindrical rod of diameter, $d_{\text{mask}} = 2.0\,\text{mm}$. By mounting the mask vertically, directly behind the collecting lens, the minimum amount of light which has passed through the filament is blocked. A simple ray tracing analysis by Talbott (1978) showed that the error associated with assuming that the path length of the light through the fluid is equal to the filament diameter is negligible.

At the onset of filament stretching, the no slip condition at the endplates and the sagging due to gravity also result in a strong axial curvature. The degree of off-axis vertical deflection of the laser beam is a complicated function of the stretch rate, the fluid properties and initial loading of the sample. This deflection cannot be corrected for optically. For a strain hardening fluid, the filament will approach an ideal cylinder at moderate strains. The effects of axial curvature are thus only present at early times. However, as the filament thins and elongates, the lateral position of the filament can shift due to air currents, slight misalignment of the rheometer or mechanical vibration. To lessen the impact of these problems a large area photodetector (3 mm$\times$3 mm) was used. The advantage of this large area photodetector is reduced sensitivity to the lateral filament location and axial curvature. The disadvantage is an enhanced sensitivity to ambient light which must then be minimized.

The output from the photodetector is split and the two outputs are fed through a low pass filter (EG&G 5113) to determine the dc intensity and through a pair of lock-in amplifiers (EG&G 7260) to measure the amplitude of the signal in phase with the fundamental frequency and out of phase with the first harmonic of the dual-crystal modulator. These measurements are recorded on a PC through a data acquisition card interfaced with LABVIEW. The intensity of the light entering the photodetector is given by

$$\begin{aligned} I(t) &= I_{\mathrm{dc}} + I_{\omega}\sin\omega t + I_{2\omega}\cos 2\omega t, \\ I_{\omega} &= 2J_1(A_c)I_{\mathrm{dc}}M_{34} = 2J_1(A_c)I_{\mathrm{dc}}\sin\delta\cos 2\chi, \\ I_{2\omega} &= 2J_2(A_c)I_{\mathrm{dc}}M_{32} = 2J_2(A_c)I_{\mathrm{dc}}[1-\cos\delta]\sin 2\chi\cos 2\chi, \end{aligned} \tag{7}$$

where M_{34} and M_{32} are the components of the Mueller matrix that correspond to the fluid filament shown in Fig. 2(a) and A_c is the amplitude of the electro-optical modulation calibrated such that the Bessel function of the first kind of order zero is equal to $J_0(A_c) = 0$ [Frattini and Fuller (1984)]. The advantage of using a modulation technique is that it is possible to calculate both the retardation, $\delta = (2\pi\Delta n' d)/\lambda_{\mathrm{light}}$, and the extinction angle, χ, simultaneously,

$$\begin{aligned} \delta &= \frac{4\pi\Delta n' R_{\mathrm{mid}}(t)}{\lambda_{\mathrm{light}}} = \cos^{-1}\left(\frac{-M_{32}^2 \pm M_{34}^2\sqrt{1-M_{34}^2-M_{32}^2}}{M_{34}^2+M_{32}^2}\right), \\ \chi &= \frac{1}{2}\cos^{-1}\left(\frac{M_{34}}{\sin\delta}\right), \end{aligned} \tag{8}$$

where the optical pathlength is equal to $d = 2R_{\mathrm{mid}}(t)$ and λ_{light} is the wavelength of the laser light. The direction of the stretch is aligned with the optics at an angle of 0° from vertical. The $I_{2\omega}$ signal will, therefore, be vanishingly small and the extinction angle is known *a priori*, $\chi = 0$. Assuming the small retardation approximation, $\delta \ll 1$, the above equations simplify to

$$M_{34} = \delta. \tag{9}$$

The Mueller matrix component M_{34} can be rewritten in terms of the light intensities entering the photodetector,

$$\delta = \frac{I_{\omega}}{\sqrt{2}J_1(A_c)I_{\mathrm{dc}}}, \tag{10}$$

TABLE I. Parameters that characterize the viscometric properties of the 0.025 wt % PS/PS solution.

Description of parameter and notation	Value
Extensibility parameter, $b = L^2$	26900
Stress-optical coefficient, C	-5.0×10^{-9} Pa^{-1}
Zero shear rate viscosity, η_0	22.75 Pa s
Solvent viscosity, η_s	21 Pa s
Elastic modulus, $n_p k_B T$	0.98 Pa
Zimm (longest) relaxation time, λ_Z	3.24 s
Average relaxation time, $\bar{\lambda}$	0.146 s
First normal stress coefficient, Ψ_{10}	6.66 Pa s^2

the square root appears in the denominator of the expression for the retardation because, in practice, I_{dc} is a root mean square (rms) voltage. The validity of the approximations leading to Eqs. (9) and (10) will be confirmed in Sec. III A.

Calibration tests showed that the minimum retardance that could be reliably and accurately resolved was $\delta_{\min} = 0.005$ rad. The value of birefringence (or elastic stress) corresponding to this value depends on the geometry of the fluid column and the wavelength of the laser. In the transient extensional measurements by Venerus *et al.* (1999) using a nonphase-modulated birefringence system, the minimum resolvable retardance was $\delta_{\min} = 0.26$ rad.

C. Test fluid

The viscoelastic test fluid used in all the experiments presented in this article consists of a 0.025 wt % solution of monodisperse polystyrene (PS) (Scientific Polymer Products, Inc.) with a molecular weight of 2.25×10^6 g/mol and polydispersity of 1.03 dissolved in oligomeric styrene (Hercules). The solution is a highly elastic dilute polymer solution or Boger fluid [Boger (1977/78)] with $c/c^* = 0.24$. A complete discussion including plots of the steady and oscillatory shear rheology of this fluid as well as the fits to Rouse–Zimm, FENE-P and Bird–DeAguiar constitutive models was published previously [Rothstein and McKinley (1999); Rothstein and McKinley (2001); Rothstein and McKinley (2002)]. For completeness, the key viscometric parameters of the PS solution are reproduced in Table I.

The rheological properties of the 0.025 wt % PS/PS are extremely sensitive to the small changes in fluid temperature that can occur due to thermal fluctuations in the laboratory test environment. To correct for these effects we employ time-temperature superposition with a shift factor determined by the Williams–Landel–Ferry (WLF) equation. A thermocouple is placed within the sample before each experiment and the temperature of the fluid is recorded. Due to the short duration of these experiments, the temperature is assumed to remain constant throughout the course of the experiment.

The Deborah number, $\mathrm{De} = \lambda/\mathcal{J}$, characterizes the relative importance of elastic effects to viscous effects in the flow. For a homogeneous extensional flow, the characteristic time scale of the kinematics is given by the inverse of the extension rate, $\mathcal{J} = \dot{\varepsilon}_0^{-1}$, while the characteristic relaxation time of the fluid is given by the longest Zimm relaxation time, $\lambda = \lambda_Z$. The Deborah number for an extensional flow thus becomes $\mathrm{De}_z = \lambda_z = \lambda_z \dot{\varepsilon}_0$. In this article, we will also be discussing results from the flow through a 4:1:4 axisymmetric contraction/expansion. In this case, the characteristic convective time scale of the flow can then be taken to be the inverse of the deformation rate in the vicinity

of the throat of the contraction plane, $\mathcal{J} = R_2/\langle v_z \rangle_2 = \dot{\gamma}^{-1}$. The choice of the appropriate average of the relaxation spectrum for a viscoelastic fluid in a contraction flow geometry has been discussed in depth by Boger *et al.* (1992) and by Rothstein and McKinley (1999). To be consistent with earlier work we will follow the choice of Rothstein and McKinley (1999), using the viscosity-weighted average relaxation time, $\bar{\lambda} = \Psi_{10}/2\eta_0$, as the characteristic relaxation time of the fluid within the axisymmetric contraction/expansion. It is important to note that the resulting relaxation times used for the extensional flow (λ_z) and contraction flow experiments ($\bar{\lambda}$) are quite different and this can lead to confusion [Boger *et al.* (1992)]. They can, however, be related quite simply for the Rouse–Zimm model,

$$\bar{\lambda} = \frac{\eta_0}{\eta_0 - \eta_s} \frac{\Sigma_{j=1}^{N_m} j^{-2(2+\sigma^*)}}{\Sigma_{j=1}^{N_m} j^{-(2+\sigma^*)}} \lambda_z = 0.045 \lambda_z, \tag{11}$$

where $\sigma^* \approx -1.40(h^*)^{0.78}$ and h^* is the hydrodynamic interaction parameter [Bird *et al.* (1987b)]. The Deborah number used for presentation of the results of the axisymmetric contraction-expansion research will thus be $De_0 = \bar{\lambda}\dot{\gamma} = \bar{\lambda}\langle v_z \rangle_2 / R_2$.

Gravitational sagging of the viscoelastic fluid filament is always a concern in extensional rheometry because it can dramatically influence experimental measurements [Stokes *et al.* (2000)]. Anna *et al.* (2001) showed that there exists a critical Deborah number below which gravitational sagging becomes important; it is

$$De_{z,\text{sag}} = \lambda_z \frac{\rho g R_0}{\eta_0}. \tag{12}$$

For the current filament stretching device and experiments using the 0.025 wt % PS/PS solution, $De_{z,\text{sag}} = 3.43$ at $T = 25\,^{\circ}\text{C}$. All the steady stretch rates presented in Sec. III A are well above the critical Deborah number. However, for the unsteady stretch profiles presented in Sec. III C, the strain rates imposed are quite small to start and increase monotonically with accumulated strain. In the worst case, the strain rate profile for a Deborah number of $De_0 = 0.5$ ($De_z = 11.1$), the first $\varepsilon = 0.5$ strain units are affected by gravitational sagging. Beyond this point, the extensional stresses in the filament grow and gravitational effects can be ignored. Thus, it is unlikely that the transient extensional rheometry measurements presented below are greatly affected by gravitational sagging of the fluid filament.

III. RESULTS AND DISCUSSION

A. Steady stretch rates

In order to validate our flow-induced birefringence experimental setup and measurement technique, a series of experiments were first performed in the filament stretching rheometer at a constant imposed stretch rate. The spectrum of stretch rates and final Hencky strains was chosen to facilitate a comparison with the existing literature [Doyle *et al.* (1998); Sridhar *et al.* (2000)].

In Fig. 3, the dc intensity, I_{dc}, of the birefringence system and the Mueller matrix coefficient, M_{34}, are plotted as a function of time for a stretching experiment at a Deborah number of $De_z = 4.1$ to a final Hencky strain of $\varepsilon_f = 5$. An inherent advantage of this ratiometric technique is the insensitivity of the Mueller matrix coefficients to variations in the pathlength and the scattering of laser light, both of which lead to dramatic changes in the dc intensity over the course of the stretch. At early times, the

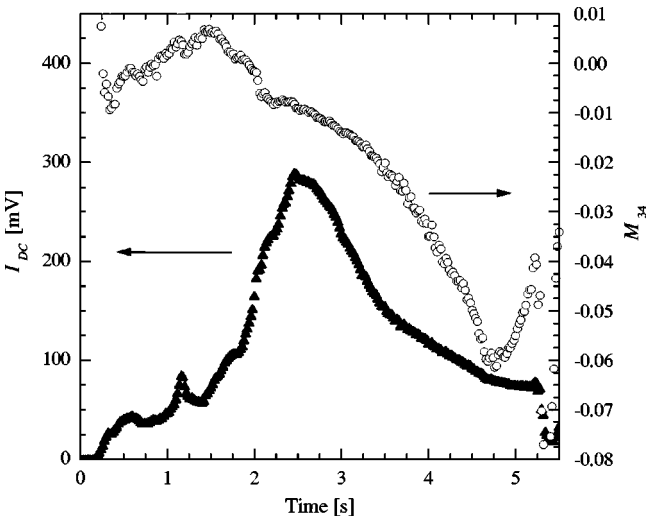

FIG. 3. Flow-induced birefringence measurements as a function of time for a strain rate of a Deborah number of $De_z = 4.1$ and a final Hencky strain of $\varepsilon_f = 5$. ▲: I_{dc}, ○: $R_\omega = M_{34}$.

signal is weak because of the axial curvature of the filament, whereas at long times the retardance may decrease due to the exponential decrease in filament radius $R_{\text{mid}}(t)$. In the present configuration, reliable birefringence measurements are not possible until a strain of $\varepsilon \approx 1$. At small strains, $\varepsilon < 1$, the filament is subject to ''reverse-squeeze flow'' which results in a very weak, positive birefringence signal. As time progresses and the accumulated Hencky strain increases to values greater than $\varepsilon > 2$, the polymer coils begin to become oriented with the flow and unravel. The birefringence signal becomes increasingly negative until flow is stopped. Observation of the chain relaxation process is then possible until the filament fails or is deflected out of the path of the laser as it drains under gravity. The small angle approximation used to derive Eq. (9) is validated by the data presented in Fig. 3 since the magnitude of M_{34} never grows larger than 0.06.

In Fig. 4, the polymeric contribution to the tensile stress and the polymer conformation is plotted against the Hencky strain for the experiment shown in Fig. 3. Also included in Fig. 4 is the theoretical prediction of the FENE-PM model [Wedgewood *et al.* (1991)]. The polymer contribution to the tensile stress is calculated by subtracting the viscous stress from Eq. (4),

$$\Delta\tau_p = \langle \tau_{zz} - \tau_{rr} \rangle - 3\eta_s \dot{\varepsilon}_0, \tag{13}$$

and the ensemble average conformational anisotropy of the polymer chains is determined by an algebraic manipulation of Eq. (6),

$$\Delta A = \frac{1}{n_p k_B T C} \left(\frac{\delta \lambda_{\text{light}}}{4\pi R_{\text{mid}}} \right). \tag{14}$$

For convenience we will refer to ΔA as the ''polymer conformation'' for the remainder of this article. The broken lines in Fig. 4 correspond to the minimum resolvable conformation computed from the minimum resolvable retardance ($\delta_{\min} = 0.005$ rad) and the minimum resolvable polymeric stress computed from the sensitivity of the force transducer ($F_{\min} = 0.01$ g),

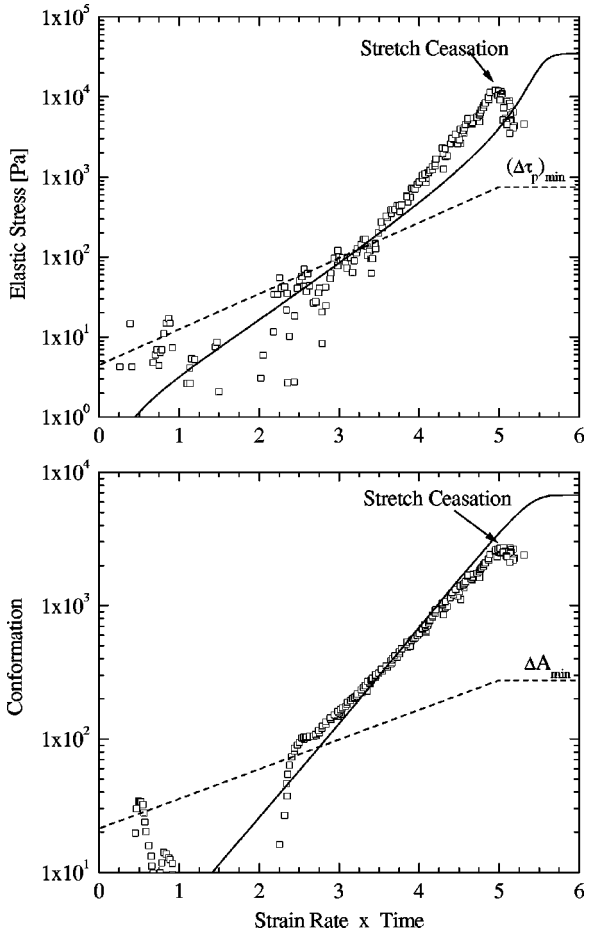

FIG. 4. Polymer contribution to the difference in elastic tensile stress and polymer coil conformation as a function of strain rate×time for a filament stretching experiment of the 0.025 wt % PS/PS solution at a Deborah number of $De_z = 4.1$ and to a final Hencky strain of $\varepsilon_f = 5$. □: Experimental data; –: FENE-PM model prediction; and - - -: the minimum resolvable conformation and elastic tensile stress calculated from calibrations of the FIB system and the force transducer.

$$(\Delta\tau_p)_{\min} = \frac{F_{\min}}{\pi R_{\text{mid}}^2(t)} - 3\,\eta_s\dot{\varepsilon}. \tag{15}$$

At small strains ($\varepsilon < 2$), the extensional stress is dominated by the Newtonian response of the oligomeric polystyrene solvent and no appreciable deformation in the polymer coils has accumulated. In fact, it is not until strain of about $\varepsilon \approx 3$ that the magnitude of the polymeric stress and conformation grows large enough to be distinguished from the solvent contribution and the noise present in the FIB optical train and the force transducer. At larger strains, the agreement between the predictions of the FENE-PM model and the experimental measurements is quite good. With the onset of strain hardening in the experimental measurements, the FENE-PM model begins to significantly underpredict the elastic stress accumulated by the fluid, but continues to accurately predict the polymer conformation. These observations are in agreement with earlier measurements [Doyle *et al.* (1998)].

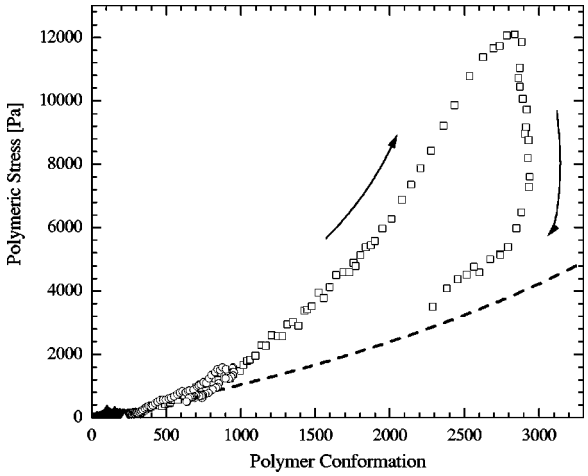

FIG. 5. Polymeric tensile stress as a function of polymer coil conformation for a filament stretching experiment of the 0.025 wt % PS/PS solution at a Deborah number of $De_z = 4.1$ ▲: Experimental data to a final Hencky strain of $\varepsilon_f = 3$; ○: experimental data to $\varepsilon_f = 4$; □: experimental data to $\varepsilon_f = 5$; and - - -: FENE-PM model predictions.

If the elastic stress, $\Delta\tau_p$, [Eq. (13)] is plotted against the polymer conformational anisotropy, ΔA, [Eq. (6)] as in Fig. 5, stress-conformation hysteresis similar to that first noted by Doyle *et al.* (1998) is observed. During startup of the stretch, the data follow the left-hand side of the loops whereas, during relaxation, the data follow the right-hand side of the hysteresis loop. The FENE-PM model cannot even capture the hysteresis loop qualitatively because it does not contain sufficient physical information about the internal configurations of the chains. In the FENE-PM model, the polymeric stress is a single-valued function of the polymer end-to-end conformation and thus the birefringence is also single valued [Doyle *et al.* (1998)]. As expected, the FENE-PM model does agree quite well with the experimental data during the latter stages of relaxation. If a conformation-dependent FENE dumbbell model [Doyle *et al.* (1998)] or the FENE-G model [Ghosh *et al.* (2001)] is used, then the hysteresis loop can be captured qualitatively, however, a quantitative prediction of the transient behavior of the hysteresis loop experimentally observed in rapid extensional flows has yet to be achieved.

Similar hysteresis loops can also be generated for filament stretching experiments performed at the same strain rate, but to different final Hencky strains. The rate at which the stress, birefringence and magnitude of the hysteresis loop grow with increasing total Hencky strain can also be appreciated by considering the data shown in Fig. 5 from fluid strains of $\varepsilon_f = 3$ and 4. The magnitude of the hysteresis loop decreases rapidly as the final strain is reduced. At the scale of Fig. 5, the data for final strain of $\varepsilon_f = 3$ are almost imperceptible. At these lower strains, the FENE-PM model predictions represent the data well during the initial onset of the stretch. The experimental data do not begin to deviate from the FENE-PM model predictions until a value of approximately $\Delta A \approx 250$ and polymeric stress of $\Delta\tau_p \approx = 250$ Pa have been reached. These values represent the upper limit for the validity of the stress-optical rule in extensional flow of this dilute polymer solution. The stress-optical rule is commonly used to convert measurements of birefringence to polymeric stress in experiments with entangled polymeric fluids where it is valid up to much larger stresses, typically $\Delta\tau_p \approx 10^5$ Pa [Janeschitz-Kriegl (1983); Venerus *et al.* (1999)]. The repeatability of these filament stretching experiments and the

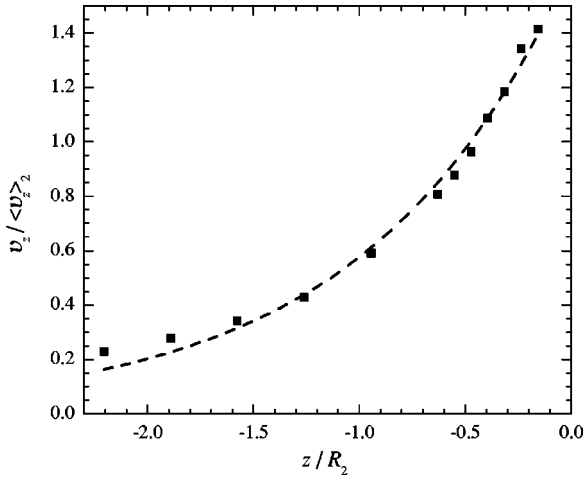

FIG. 6. LDV measurements of the centerline velocity profile upstream of a 4:1:4 axisymmetric contraction/expansion for a Deborah number of $De_0 = 1.5$. ■: Experimental data and - - -: fit of the form $\nu_z / \langle \nu_z \rangle_2 = B \exp(-C|z|/R_2)$.

flow-induced birefringence system in general is demonstrated in Fig. 5. All three experiments superimpose quite nicely, and follow the same trajectory during the initial stages of stretching and the same relaxation dynamics in the last stages of the polymeric stress relaxation process.

B. 4:1:4 contraction–expansion centerline profiles

It has been conjectured in the literature that the stress-conformation hysteresis observed in homogeneous uniaxial elongation may significantly contribute to the enhanced drop in pressure through axisymmetric contractions and the enhanced drag observed in other complex flows [Chmielewski *et al.* (1990); Solomon and Muller (1996); Rothstein and McKinley (1999); Rothstein and McKinley (2001)]. However, if we take the 4:1:4 contraction/expansion, for example, the total Hencky strain accumulated by a material element flowing along the centerline is only $\varepsilon = 2.77$. At these low strains, a constant stretch rate experiment shows very little hysteresis as indicated in Fig. 5. Simulations of time-varying extensional flows [Hernandez Cifre and de la Torre (1998)] suggest that inhomogeneous uniaxial extension (corresponding to the strain rate profile a material element experiences as it travels along the centerline towards the contraction plane) may still result in substantial hysteresis. We now proceed to investigate this possibility experimentally.

In a previous paper, we reported measurements of the axisymmetric flow-induced birefringence along the centerline of the 4:1:4 contraction/expansion using the same 0.025 wt % polystyrene Boger fluid [Rothstein and McKinley (2000)]. As expected, these birefringence measurements demonstrated significant orientation and elongation of the polymer chain upstream of the contraction followed by rapid relaxation downstream. However, to gain more physical insight into this complex flow, it would be informative to simultaneously measure the stress and birefringence in the fluid passing through the contraction-expansion geometry. Unfortunately, the only available measure of stress in the contraction/expansion is the global drop in pressure which is, in fact, the quantity into which we hope to gain some physical insight. Instead of measuring the stress and bire-

TABLE II. Values for the exponential fit to the centerline velocity profiles upstream of 4:1:4 axisymmetric contraction expansion.

Deborah number	B	C	$\tilde{t}_0$	$\tilde{z}_0$
0.5	1.694	0.849	4.697	−2.250
1.0	1.587	0.922	4.470	−2.037
1.5	1.665	1.048	4.000	−1.854
2.5	1.585	0.752	5.204	−2.427
3.5	1.750	0.557	7.468	−3.562

fringence of a fluid element within the contraction-expansion flow, we isolate a representative fluid element and expose it to the identical kinematic history using the filament stretching rheometer.

As indicated in Fig. 1, fluid elements traveling along the centerline of the contraction/expansion are exposed to rapid transient inhomogeneous extensional flow. To determine the exact strain rate profile experienced by fluid elements, we reanalyze pointwise measurements of the axial velocity reported previously [Rothstein and McKinley (2001)] are analyzed. The centerline LDV measurements upstream of the 4:1:4 axisymmetric contraction/expansion at a Deborah number of $De_0 = \bar{\lambda}\dot{\gamma} = \bar{\lambda}\langle v_z\rangle_2/R_2 = 1.5$ are shown in Fig. 6. The velocities are nondimensionalized by the average velocity within the contraction, $\tilde{v} \equiv v_z/\langle v_z\rangle_2 = v_z/(Q/\pi R_2^2)$, the distance upstream is nondimensionalized by the radius of the throat, $\tilde{z} \equiv z/R_2$, and the time is nondimensionalized by a convective time scale, $\tilde{t} \equiv t\langle v_z\rangle_2/R_2$. For a Newtonian fluid element undergoing creeping flow (Reynolds number, $\mathrm{Re} \ll 1$) through an orifice with infinite aspect ratio, Sampson found that the centerline velocity is given by $\tilde{v} = 3/[2(\tilde{z}^2+1)]$ [Happel and Brenner (1965)]. However, the experimental data show that the centerline velocity profiles vary slightly as the flow rate (and the Deborah number) is increased. A suitable Eulerian velocity profile that captures the dependence observed experimentally is given by

$$\tilde{v}(\tilde{z}) = v_\infty + Be^{-C|\tilde{z}|} \tag{16}$$

for all Deborah numbers up to $De_0 = 4.5$. In Eq. (16), v_∞, B and C are fitting parameters which vary with the Deborah number. The value of v_∞ corresponds to twice the dimensionless average velocity upstream of the contraction, $v_\infty = 2/\beta^2$. However for the purpose of converting Eq. (16) to a Lagrangian velocity profile analytically, we subtract v_∞ from the measured data and fit the data to determine values of B and C. Table II lists the values of the constants used to fit the velocity profiles at various Deborah numbers.

To calculate the proper velocity profile of the filament stretching rheometer endplates, we must first determine the strain rate profile of a fluid element traveling along the centerline of the contraction/expansion. By integrating Eq. (16), the Lagrangian position of a fluid element, $\tilde{Z}(\tilde{z}_0,\tilde{t})$, can be determined as a function of time for $\tilde{Z} \leqslant 0$,

$$\tilde{Z} = -\frac{1}{C}\ln[BC(\tilde{t}_0 - \tilde{t})], \tag{17}$$

where $\tilde{t}_0$ is a dimensionless time constant that is related to the initial dimensionless upstream position of the fluid element, $\tilde{z}_0$,

$$\tilde{t}_0 = \frac{1}{BC}e^{-C\tilde{z}_0}. \tag{18}$$

Throughout the course of these experiments, z_0 will be set such that $\tilde{v}(\tilde{z}_0) = 2/\beta^2$. Equation (17) is then differentiated to determine the velocity of the particle as a function of time,

$$\tilde{v}(\tilde{z}_0,\tilde{t}) = \frac{1}{C(\tilde{t}_0-\tilde{t})}. \tag{19}$$

The dimensionless strain rate of the fluid particle as a function of time thus becomes

$$\tilde{\dot{\varepsilon}}(\tilde{z}_0,\tilde{t}) = \frac{d\tilde{v}}{d\tilde{z}} = \frac{d\tilde{v}}{d\tilde{t}}\frac{d\tilde{t}}{d\tilde{z}} = \frac{1}{(\tilde{t}_0-\tilde{t})}, \tag{20}$$

while the total accumulated strain as a function of time is given by

$$\varepsilon = \int_0^{\tilde{t}} \tilde{\dot{\varepsilon}} d\tilde{t}' = \ln\left(\frac{\tilde{t}_0}{\tilde{t}_0-\tilde{t}}\right). \tag{21}$$

The experiments are terminated when the Hencky strain accumulated by the particle equals the total strain accumulated within the contraction. For a 4:1:4 contraction, $\varepsilon_f = 2\ln(\beta) = 2.77$. Hence, the total time for the stretch, $\tilde{t}_f$, can be expressed as a function of the contraction ratio β and the time constant $\tilde{t}_0$,

$$\tilde{t}_f = \tilde{t}_0\left(1-\frac{1}{\beta^2}\right). \tag{22}$$

From Eq. (22) it is evident that the extension rate would diverge, $\tilde{\dot{\varepsilon}} \to \infty$, as $\tilde{t} \to \tilde{t}_0$. However, since $\tilde{t}_f < \tilde{t}_0$ we find that the maximum strain rate is given by $\tilde{\dot{\varepsilon}}_{\max} = \tilde{\dot{\varepsilon}}(t_f) = \beta^2/\tilde{t}_0$. From Table II, it can be seen that $4 \leqslant \tilde{t}_0 < 8$ and for a 4:1:4 contraction ($\beta^2 = 16$) thus we find that the maximum extension rate at the contraction plane is between two to four times as large as the characteristic scale $\langle v_z\rangle/R_2$ used to nondimensionalize the strain rate.

Finally, we must convert the desired strain rate given by Eq. (20) into a commanded position profile for the filament stretching rheometer. In the filament stretching rheometer, the total Hencky strain for a ideal uniaxial deformation is given by

$$\varepsilon = \ln\left(\frac{L(t)}{L_0}\right). \tag{23}$$

Substituting into Eq. (21) and exponentiating both sides, we can calculate the appropriate endplate separation as

$$L(t) = L_0\left(\frac{\tilde{t}_0}{\tilde{t}_0-\tilde{t}}\right), \tag{24}$$

and the velocity profile of the endplate required to simulate the transient inhomogeneous uniaxial extension experienced by a fluid element traveling along the centerline upstream of a 4:1:4 axisymmetric contraction/expansion is then (in dimensional form),

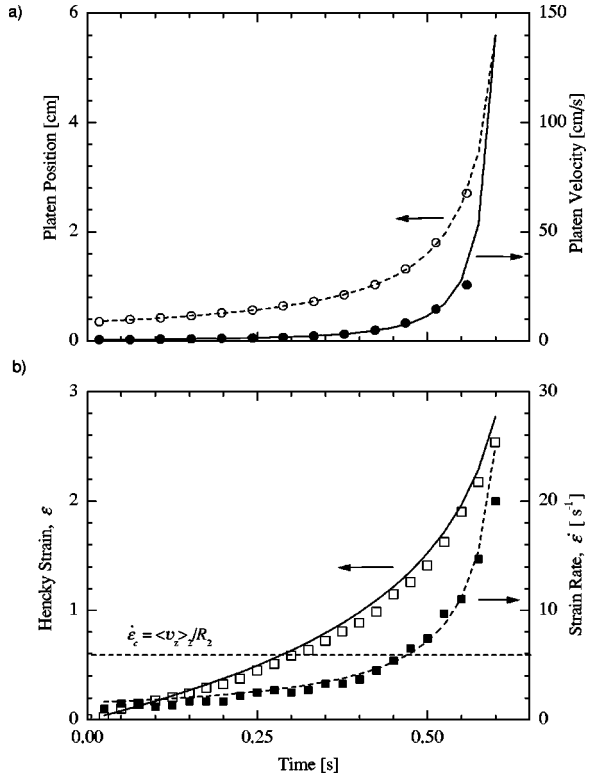

FIG. 7. Deformation profiles of a fluid filament being stretched simulating the centerline profile into 4:1:4 contraction/expansion at a Deborah number of $De_0 = 1.5$. Included in (a) - - - endplate commanded position; –: endplate commanded velocity; ● experimental endplate position; and ○: experimental endplate velocity. Included - - - in (b) are commanded strain rate; –: commanded total accumulated strain; ■: experimental strain rate; and □: experimental strain.

$$\dot{L}(t) = L_0 \frac{\langle v_z \rangle_2}{R_2} \frac{\tilde{t}_0}{\left(\tilde{t}_0 - \dfrac{\langle v_z \rangle_2 t}{R_2} \right)^2}. \tag{25}$$

The calculated profiles corresponding to a Deborah number of $De_0 = 1.5$ are shown in Fig. 7 in dimensional form. Note that the strain rate monotonically increases in time which is in agreement with Eq. (20). For comparison, the average or characteristic stretch rate, $\dot{\varepsilon}_c = \langle v_z \rangle / R_2$, is also shown by the broken line.

Upon completion of the stretch at time $\tilde{t}_f$, the platens are stopped and polymeric stress relaxation of the fluid filament is observed. Although the strain rate profile during the imposed stretch will accurately mimic the conditions upstream of contraction/expansion, the relaxation process does not correspond to the region of biaxial compression actually experienced downstream of the expansion. Theoretically, the downstream compression could be imposed by the filament stretching device, however, in practice the slender fluid filament will buckle under such compressive loading.

The flow through an axisymmetric contraction/expansion is an inhomogeneous transient extensional flow in which the extensional deformation is localized to a small region on the centerline near the contraction plane. At very high deformation rates this can lead

to chain scission of polystyrene molecules [Clay and Koelling (1997)], however, we operate at much lower characteristic deformation rates and lower maximum stresses. No molecular degradation was noted, however fluid samples were only passed through the contraction/expansion a maximum of 30 times at various Deborah numbers.

C. Measurement of inhomogeneous extensional flow into 4:1:4 contraction/expansion

Using the parameters that characterize the velocity profiles in Table II and the master curve inversion procedure [Anna *et al.* (1999); Orr and Sridhar (1999)] it is now possible to program a desired inhomogeneous velocity profile and directly observe the polymeric stress growth and polymer conformation of a fluid element traveling along the centerline into an axisymmetric contraction/expansion. The aim of these experiments is to explain the additional extra drop in pressure observed in the flow of elastic liquids through an energy loss argument associated with stress-conformation hysteresis [Doyle *et al.* (1998)]. Therefore, all the filament stretching results presented in this section will compare the polymeric tensile stress with the average conformation of the polymer chain.

Superimposed over the calculated profiles presented in Fig. 7 are the platen position, platen velocity, filament strain and filament strain rate achieved experimentally. The agreement is found to be quite good and the strain profile of a fluid element traveling along the centerline upstream of a 4:1:4 contraction/expansion at a Deborah number of $De_0 = 1.5$ can thus be effectively reproduced within the filament stretching rheometer. In Fig. 8(a), the polymeric stress and polymer conformation results from this experiment are shown as a function of time. At small strains and times, the polymeric stress and polymer conformation remain undetectable within the experimental resolution of the instrument. At times greater than approximately $t > 0.5$ s, corresponding to an instantaneous strain rate greater than approximately $\dot{\varepsilon} > 8\ \mathrm{s}^{-1}$, both the polymeric stress and the polymer conformation begin to grow rapidly. The chains are aligned with the flow direction, but not significantly extended. The maximum polymer conformation measured for the experiment is only $\Delta A = 375$, just 4% of the maximum extension of the polymer coil. Upon cessation of the flow at $t_f = 0.6$ s, both the polymeric stress and polymer conformation decay rapidly; the polymer conformation anisotropy relaxes almost exponentially with a time constant λ_Z as expected [Doyle *et al.* (1998)], whereas initial decay of the polymeric stress is significantly more rapid. If time is eliminated from Fig. 8(a) and the polymeric stress is plotted as a function of polymer conformation, a small hysteresis loop is observed. It is clear from Fig. 8(b) that the magnitude of this hysteresis loop is significantly smaller than those observed and discussed in Sec. III B, but it is still clearly measurable.

The series of experiments outlined in Table II were performed for strain rate profiles equivalent to those observed along the centerline upstream of a 4:1:4 contraction/expansion at Deborah numbers between $0.5 \leqslant De_0 \leqslant 3.5$. Representative plots of the stress-conformation hysteresis loops for each of these Deborah numbers are presented in Fig. 9. For clarity, we have omitted the experimental data at small strains when the optical and mechanical measurements are below their respective resolution limits. As shown in Fig. 9(a), at a Deborah number of $De_0 = 0.5$ (corresponding to $De_z = \lambda_z \dot{\varepsilon}_c = 11.1$ based on the characteristic strain rate) very little polymeric tensile stress or polymer stretch is generated. The hysteresis loop associated with this stretch profile is small in comparison to the data presented in Fig. 8. As the Deborah number is increased, the differences in polymeric stress, polymer conformational anisotropy and magnitude of the hysteresis loop all increase. The initial stretch rates at the beginning of

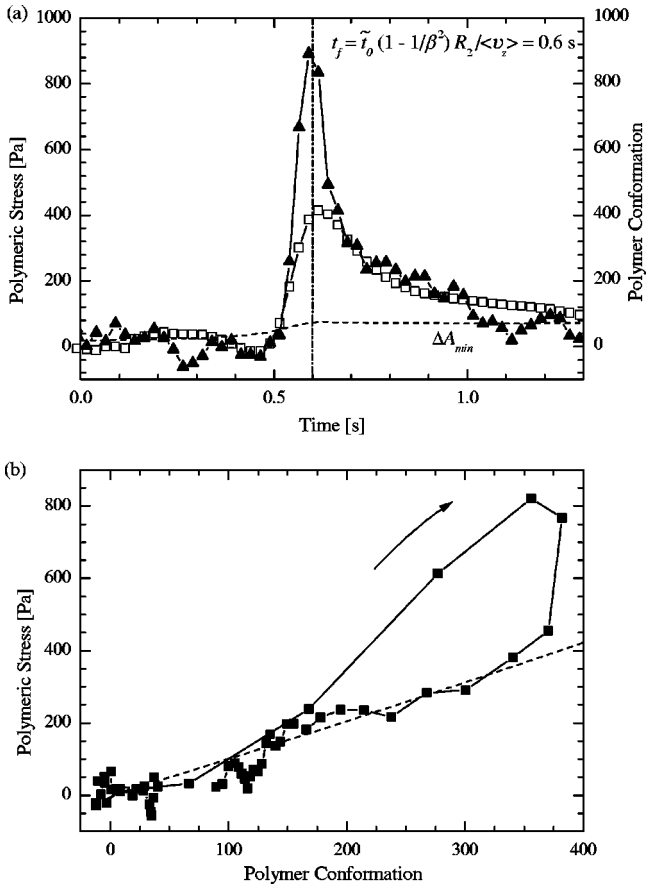

FIG. 8. Polymeric tensile stress and anisotropic coil conformation for the inhomogeneous uniaxial stretch profile corresponding to the centerline strain rate profile upstream of 4:1:4 contraction/expansion at a Deborah number of $De_0 = 1.5$. Included in (a) are ▲: the polymeric stress and □: polymer conformation as a function of time and in (b) ■: the experimental polymeric stress as a function of conformation, as well as - - -: the FENE-PM model predictions.

the low Deborah number experiments are not large enough to result in significant chain orientation or unraveling. For these inhomogeneous filament stretching experiments, the extension rates applied grow with an increase in Deborah number, but the total amount of accumulated Hencky strain is fixed at $\varepsilon_D = 2.77$. Beyond a Deborah number of $De_0 = 1.5$, a plateau of $\Delta A \approx 450$ in polymer chain deformation is observed even as the polymeric stress continues to grow.

IV. DISCUSSION AND CONCLUSIONS

The polymeric stress versus polymer conformation plots presented in Figs. 8 and 9 are analogous to the stress versus strain plots often used to investigate material hysteretic properties in viscoelastic solid mechanics. In both cases, the area enclosed by the hysteresis loop has units of energy per unit volume. In solid mechanics, this energy represents the amount of work required to plastically deform a nonHookean elastic solid. For a viscoelastic fluid, it represents the work done by purely dissipative contributions to the stress coupled to the nonequilibrium kinematics of the extensional flow. To quantify the

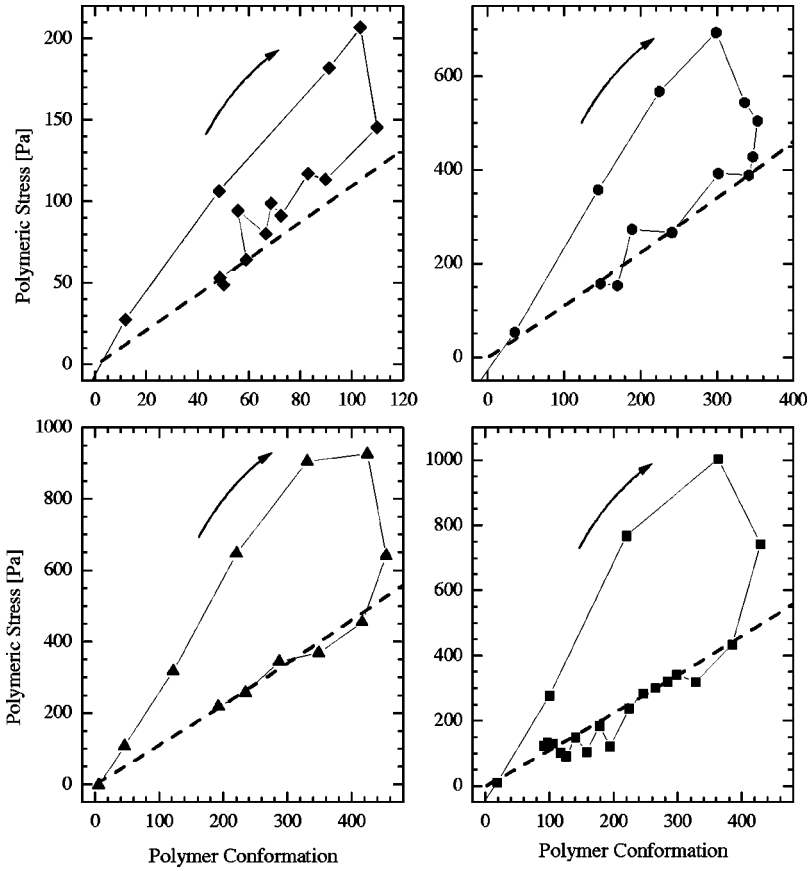

FIG. 9. Polymeric tensile stress as a function of polymer coil conformation for the 0.025 wt % PS/PS solution for type III filament stretching experiments corresponding to the centerline strain rate profile upstream of a 4:1:4 contraction/expansion at several different Deborah numbers. (a) ♦: $De = 0.5$; (b) ●: $De = 1.0$; (c) ▲: $De = 2.5$; (d) ■: $De = 3.5$; - - -: the FENE-PM model predictions.

energy dissipation as a function of Deborah number, the polymeric tensile stress is numerically integrated over the hysteresis loop,

$$E_D = \oint \frac{\Delta \tau_p}{n_p k_B T} \mathrm{d}\Delta A. \tag{26}$$

The energy dissipation per unit volume is made dimensionless by dividing the elastic tensile stress by the elastic modulus of the test fluid. If the experimental data do not continue toward zero polymer conformation during the relaxation process, the hysteresis loop is closed using the FENE-PM model predictions from the last data point back to the origin.

In Fig. 10, the dissipative energy loss, E_D, is plotted against the Deborah number of the filament stretching experiments that emulate the centerline strain rate profile upstream of a 4:1:4 contraction/expansion. The results for each Deborah number were repeated many times and the average value of the dissipative energy loss is plotted along with the standard error in these measurements which is typically on the order of $\pm 15\%$. This

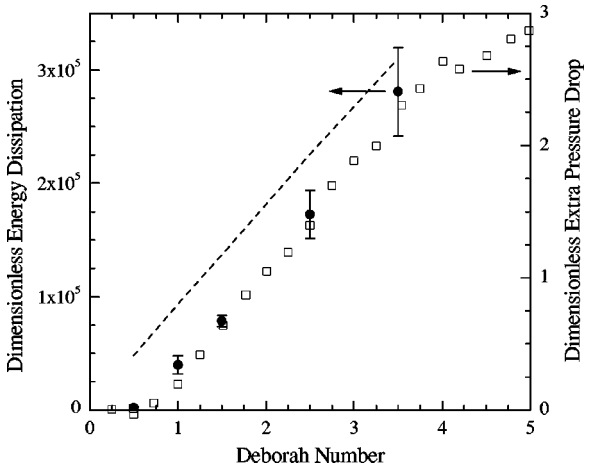

FIG. 10. Dimensionless energy dissipation and extra drop in pressure as a function of the Deborah number of the centerline stretch rate profile into 4:1:4 contraction/expansion for the 0.025 wt % PS/PS solution. ●: The experimental dimensionless energy dissipation; - - -: the Rallison dissipative stress model predictions for dimensionless energy dissipation; and □: the experimental dimensionless extra drop in pressure.

measurement error results from noise in the birefringence and force measurements as well as from the profile error associated with the type II–type III master curve inversion procedure.

An excellent fit to the measured extra dissipation arising from the hysteresis loop can be achieved using a linear fit of the form $E_D = 8.9\times10^4\ (De_0 - 0.48)$. Using this fit we can begin to assess the predictions of some recent constitutive models. Take, for example, the Rallison dissipative stress model [Rallison (1997)]. The form of the model is similar to a FENE-P model except that the polymeric stress term now has an additional purely dissipative component which relaxes immediately after cessation of the flow. The constitutive equation is written as

$$\begin{aligned} \lambda_z \mathbf{A}_{(1)} &= -[f(\mathrm{tr}\,\mathbf{A})\mathbf{A} - \mathbf{I}], \\ \tau_p &= \frac{\eta_p}{\lambda_z}[f(\mathrm{tr}\,\mathbf{A})\mathbf{A} - \mathbf{I}] + \eta_2\left(\frac{\mathbf{A}:\dot{\gamma}}{\mathrm{tr}\,\mathbf{A}}\right)\mathbf{A}, \\ f(\mathrm{tr}\,\mathbf{A}) &= \left(1 - \frac{\mathrm{tr}\,\mathbf{A}}{L^2}\right)^{-1}, \end{aligned} \tag{27}$$

where the subscript (1) indicates the usual upper convected derivative. The model predictions were calculated for the exact stretch profiles used in these filament stretching experiments through numeric integration of Eq. (27) and are plotted alongside the experimental data in Fig. 10 for a value of $\eta_2 = 0.15\,\eta_p = 0.26$ Pa s. The value of η_2 was selected to match the slope of the experimental data at large Deborah numbers. For strong deformations, the dissipative component of the polymeric stress in Eq. (27) (and therefore the total energy dissipation as well) increases approximately linearly with the Deborah number, $E_{D,\mathrm{Rallison}} \cong 9\times10^4\ (De_0 - 0.02)$. However, for the weak deformations associated with extensional flows at small Deborah numbers, the predictions of the Rallison model do not follow the same simple linear relation. Our numerical simulations show that, for the Rallison model, the total energy dissipation becomes negligible at a Deborah

number of approximately $De_0 \approx 0.02$ which corresponds to a Deborah number based on the Zimm relaxation time of approximately $De_Z = \lambda_Z \langle v_z \rangle_2 / R_2 \approx 0.5$. The general linear form of the energy dissipation is captured by this simple dissipative stress model, yet it is unable to quantitatively match the experimental data at any Deborah numbers.

For comparison, we also show in Fig. 10 the dimensionless extra drop in pressure measured for the flow of the same polymer solution through a 4:1:4 axisymmetric contraction/expansion. This extra drop in pressure is defined as

$$\Delta P_{\text{extra}} = \frac{[\Delta P(De, \dot{\gamma}) - \Delta P(De = 0, \dot{\gamma})]}{\Delta P(De = 0, \dot{\gamma})}, \tag{28}$$

and was originally reported by Rothstein and McKinley (2001) in an alternate form. These pressure-drop measurements were taken across a 4:1:4 contraction/expansion and thus contain information about the energy dissipation resulting from both the upstream and downstream kinematics. Even though we cannot replicate the relaxation profile downstream of the re-expansion; the correlation between the microscopic and macroscopic measurements is quite striking. For the flow through a 4:1:4 axisymmetric contraction/expansion, no additional drop in pressure was observed until a Deborah number of $De_0 \approx 0.5$ was reached. This critical Deborah number agrees quite well with the onset conditions for the onset of stress-conformation hysteresis and significant energy dissipation.

A careful re-examination of Figs. 8 and 9 shows that the forms of all the hysteresis loops are similar. This suggests that there might be a way to collapse all the experimental data onto a single master curve. To accomplish this we replot the hysteresis loops presented in Fig. 9, normalizing the polymeric conformation with the maximum experimentally measured polymeric conformation and define $\Delta\bar{A} = \Delta A / \Delta A_{\max}$. We make the polymeric stress dimensionless by dividing by the stress predicted by the FENE-P model at the maximum experimentally measured polymeric conformation,

$$\Delta\bar{\tau}_p = \frac{\Delta\tau_p}{\left\{\dfrac{n_p k_B T \Delta A_{\max}}{(1 - \text{tr}\{A_{\max}\}/L^2)}\right\}}. \tag{29}$$

The results of this rescaling are shown in Fig. 11. Although the profiles are indeed of the same general form, they clearly demonstrate growth in the hysteretic behavior with an increase in Deborah number. These results also suggest a possible robust dimensionless measure of the hysteretic behavior for a given trajectory. This measure is generated by the ratio of the area contained by the hysteresis loop to the area under the quasistatic FENE-P force extension curve. The area under the FENE-P force extension curve corresponds to the elastic work done (and stored entropically) to stretch a FENE-P dumbbell to a deformation of $\Delta A_{\max}$. The resulting measure of hysteresis is thus given by the following energy ratio:

$$H = \frac{\oint \Delta\tau_p \, \mathrm{d}\Delta A}{\int \Delta\tau_p^{\text{FENE}} \mathrm{d}\Delta A} \cong \frac{\oint \Delta\tau_p \, \mathrm{d}\Delta A}{-n_p k_B T L^4 \left\{ \ln\left(1 - \dfrac{\Delta A_{\max}}{L^2}\right) + \dfrac{\Delta A_{\max}}{L^2} \right\}}. \tag{30}$$

For moderate deformations, the FENE-P curve is approximately linear and the denominator of Eq. (30) reduces to $\frac{1}{2} n_p k_B T \Delta A_{\max}^2$. Rescaling the energy dissipation in this way

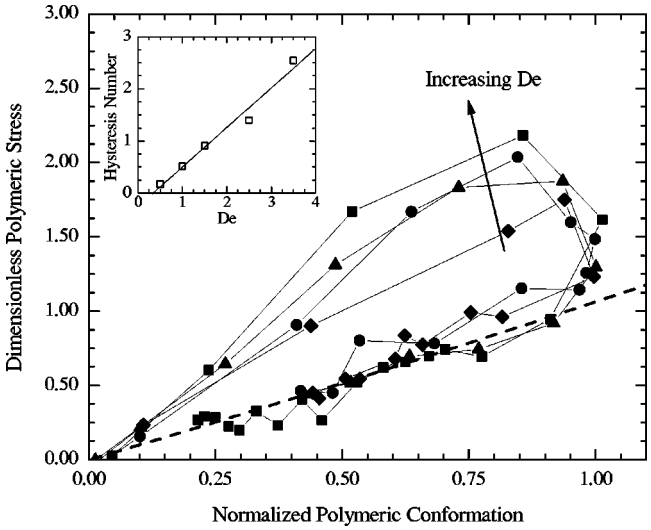

FIG. 11. Dimensionless polymeric tensile stress as a function normalized polymer coil conformation for the 0.025 wt % PS/PS solution for type III experimental stretch of the centerline strain rate profile upstream of 4:1:4 contraction/expansion at several different Deborah numbers. (a) ♦: $De = 0.5$; (b) ●: $De = 1.0$; (c) ▲: $De = 2.5$; (d) ■: $De = 3.5$; and - - -: the FENE-PM model predictions. The inset shows growth of the hysteresis number as a function of the Deborah number (□) and the linear fit to the experimental data –.

leads to a hysteresis number that increases approximately linearly from $H = 0.2$ to 2.6 with an increase in Deborah number as shown in the inset of Fig. 11.

By tailoring the strain rate profile within the filament stretching rheometer to reproduce the extensional flow along the centerline upstream of 4:1:4 contraction/expansion, it is possible to simultaneously measure the polymeric stress and polymer conformation of a polymer coil undergoing a time-varying extensional deformation characteristic of a prototypical complex flow. The resulting measurements of stress-conformation hysteresis lead us to conclude that the additional energy loss of a polymeric solution in fast transient extension is directly related to the additional drop in pressure and drag coefficients observed for these same fluids in complex flows. The form of the transient evolution in the hysteresis loops shown in Figs. 9 and 11 can also help rationalize recent observations of highly elastic polymer solutions in other complex flows. In a recent paper, Nigen and Walters (2002) showed that although there is a large enhanced drop in pressure in flow through axisymmetric contractions, the corresponding flow (at the same nominal deformation rate) in a planar contraction has a pressure drop-flow rate relationship that is indistinguishable from that of a Newtonian fluid of the same viscosity [corresponding to $\Delta P_{\text{extra}} = 0$ in Eq. (28)]. In a 4:1 planar contraction, the total strain accumulated is given by $\varepsilon = \ln \beta \simeq 1.38$. Our measurements in Figs. 9 and 11 show that at such small strains the additional polymeric stress resulting from coil-stretch hysteresis is extremely small and thus no additional macroscopic drop in pressure should be expected. Even in planar contractions with much larger contraction ratios, the different functional form of the kinematics upstream of the contraction plane will result in a much more gradual acceleration of the fluid element and less conformational hysteresis.

If one hopes to accurately model a polymer solution in complex flows, it is therefore essential that the constitutive model chosen can quantitatively reproduce the response of the polymeric stress and polymer conformation in both homogeneous and inhomogeneous transient extensional flows. With current closed-form bead-spring constitutive

models this is not yet possible. Additional microstructural information is required to capture the physics of a polymer coil unraveling in a strong flow. The challenge is creating such a model that is also suitably frame invariant and history dependent yet computationally tractable. A recent innovation was proposed by Ghosh *et al.* (2002) who incorporated a rate-dependent finite extensibility parameter into a standard FENE model. The preliminary results are encouraging in transient extensional flows [Joo *et al.* (2001)], but more work and further refinement of the model remain to be done.

ACKNOWLEDGMENTS

This research was sponsored by the NASA Microgravity Fluid Physics Program under Grant No. NCC3-610. The authors would like to thank the anonymous referees for their suggestions regarding the form of the hysteresis loop in Fig. 11.

References

Agarwal, U. S., ''Effect of initial conformation, flow strength and hydrodynamic interaction on polymer molecules in extensional flows,'' J. Chem. Phys. **113**, 3397–3403 (2000).

Anna, S. L. ''Filament stretching of model elastic liquids,'' PhD thesis, Harvard University, Cambridge, MA, 2000.

Anna, S. L., C. B. Rogers, and G. H. McKinley, ''On controlling the kinematics of a filament stretching rheometer using a real-time active control mechanism,'' J. Non-Newtonian Fluid Mech. **87**, 307–335 (1999).

Anna, S. L., G. H. McKinley, D. A. Nguyen, T. Sridhar, S. J. Muller, J. Huang, and D. F. James, ''An interlaboratory comparison of measurements from filament stretching rheometers using common test fluids,'' J. Rheol. **45**, 83–114 (2001).

Binding, D. M., and K. Walters, ''On the use of flow through a contraction in estimating the extensional viscosity of mobile polymer solutions,'' J. Non-Newtonian Fluid Mech. **30**, 233–250 (1988).

Bird, R. B., R. C. Armstrong, and O. Hassager, *Dynamics of Polymeric Liquids*: Vol. 1, Fluid Mechanics (Wiley, New York, 1987).

Bird, R. B., C. F. Curtiss, R. C. Armstrong, and O. Hassager, *Dynamics of Polymeric Liquids*: Vol. 2, Kinetic Theory (Wiley, New York, 1987).

Boger, D. V., ''A highly elastic constant-viscosity fluid,'' J. Non-Newtonian Fluid Mech. **3**, 87–91 (1977/78).

Boger, D. V., ''Viscoelastic flows through contractions,'' Annu. Rev. Fluid Mech. **19**, 157–182 (1987).

Boger, D. V., M. J. Crochet, and R. A. Keiller, ''On viscoelastic flows through abrupt contractions,'' J. Non-Newtonian Fluid Mech. **44**, 267–279 (1992).

Chmielewski, C., K. L. Nichols, and K. Jayaraman, ''A comparison of the drag coefficients of spheres translating in corn-syrup-based and polybutene-based Boger fluids,'' J. Non-Newtonian Fluid Mech. **35**, 37–49 (1990).

Clay, J. D., and K. W. Koelling, ''Molecular degradation of concentrated polystyrene solutions in a fast transient extensional flow,'' Polym. Eng. Sci. **37**, 789–800 (1997).

Cogswell, F. N., ''Measuring the extensional viscosity of polymer melts,'' Polym. Eng. Sci. **12**, 64–73 (1972).

Doyle, P. S., E. S. G. Shaqfeh, G. H. McKinley, and S. H. Spiegelberg, ''Relaxation of dilute polymer solutions following extensional flow,'' J. Non-Newtonian Fluid Mech. **76**, 79–110 (1998).

Frattini, P. L., and G. G. Fuller, ''A note on phase-modulated flow birefringence,'' J. Rheol. **28**, 61–70 (1984).

Fuller, G. G., *Optical Rheometry of Complex Fluids* (Oxford University Press, New York, 1995).

Ghosh, I., G. H. McKinley, R. A. Brown, and R. C. Armstrong, ''Deficiencies of FENE dumbbell models in describing the rapid stretching of dilute polymer solutions,'' J. Rheol. **45**, 721–758 (2001).

Ghosh, I., Y. L. Joo, G. H. McKinley, R. A. Brown, and R. C. Armstrong, ''A new model for dilute polymer solutions in flows with strong extensional components,'' J. Rheol. **46**, 1057–1089 (2002).

Happel, J., and H. Brenner, *Low Reynolds Number Hydrodynamics* (Prentice-Hall, Englewood Cliffs, NJ, 1965).

Hernandez Cifre, J. G. and J. G. de la Torre, ''Simulation of polymers in dilute solution under extensional flow,'' J. Non-Cryst. Solids **235–237**, 717–722 (1998).

Janeschitz-Kriegl, H., *Polymer Melt Rheology and Flow Birefringence* (Springer, Berlin, 1983).

Joo, Y. L., S. D. Phillips, J. P. Rothstein, G. H. McKinley, R. C. Armstrong, and R. A. Brown, ''Use of an adaptive length scale model in the simulation of flow of a viscoelastic fluid through an axisymmetric contraction-expansion,'' Society of Rheology 73rd Annual Meeting, Bethesda, MD, 2001.

Kolte, M. I., H. K. Rasmussen, and O. Hassager, ''Transient filament stretching rheometry. II. Numerical simulation,'' Rheol. Acta **36**, 285–302 (1997).

Li, L., R. G. Larson, and T. Sridhar, ''Brownian dynamics simulations of dilute polystyrene solutions,'' J. Rheol. **44**, 291–322 (2000).

Li, J.-M., W. R. Burghardt, B. Yang, and B. Khomami, ''Flow birefringence and computational studies of a shear-thinning polymer solution in axisymmetric stagnation flow,'' J. Non-Newtonian Fluid Mech. **74**, 151–193 (1998).

Mackey, J. R., K. K. Das, S. L. Anna, and G. H. McKinley, ''A compact dual-crystal modulated birefringence-measurement system for microgravity applications,'' Meas. Sci. Technol. **10**, 946–955 (1999).

McKinley, G. H., and T. Sridhar, ''Filament stretching rheometry,'' Annu. Rev. Fluid Mech. **34**, 375–415 (2002).

Nguyen, T. Q., and H.-H. Kausch, *Flexible Polymer Chains in Elongational Flow: Theory and Experiment* (Springer, Berlin, 1999).

Nguyen, T. Q., R. Porouchani, and H.-H. Kausch, ''Birefringence of dilute PS solutions in abrupt contraction flow,'' in: *Flexible Polymer Chains in Elongational Flow: Theory and Experiment*, edited by T. Q. Nguyen and H. H. Kausch (Springer, Berlin, 1999), pp. 185–228.

Orr, N. V., and T. Sridhar, ''Probing the dynamics of polymer solutions in extensional flow using step strain rate experiments,'' J. Non-Newtonian Fluid Mech. **82**, 203–232 (1999).

Quinzani, L. M., R. C. Armstrong, and R. A. Brown, ''Use of coupled birefringence and LDV studies of flow through a planar contraction to test constitutive equations for concentrated polymer solutions,'' J. Rheol. **39**, 1201–1228 (1995).

Rajagopalan, D., ''Computational analysis of techniques to determine extensional viscosity from entrance flows,'' Rheol. Acta **39**, 138–151 (2000).

Rallison, J. M., ''Dissipative stresses in dilute polymer solutions,'' J. Non-Newtonian Fluid Mech. **68**, 61–83 (1997).

Rothstein, J. P., and G. H. McKinley, ''Extensional flow of a polystyrene Boger fluid through a 4:1:4 axisymmetric contraction/expansion,'' J. Non-Newtonian Fluid Mech. **86**, 61–88 (1999).

Rothstein, J. P., and G. H. McKinley, ''Axisymmetric flow-induced birefringence measurements for the flow of a polystyrene Boger fluid into an abrupt contraction-expansion,'' Proceedings of the XIIIth International Congress on Rheology, 2000, Vol. 2, pp. 282–284.

Rothstein, J. P., and G. H. McKinley, ''The axisymmetric contraction-expansion: The role of extensional rheology on vortex growth dynamics and the enhanced pressure drop,'' J. Non-Newtonian Fluid Mech. **98**, 33–63 (2001).

Rothstein, J. P., and G. H. McKinley, ''A comparison of the stress and birefringence growth of dilute, semi-dilute and concentrated polymer solutions in uniaxial extensional flows,'' J. Non-Newtonian Fluid Mech. (in press, 2002).

Sizaire, R., G. Lielens, I. Jaumain, R. Keunings, and V. Legat, ''On the hysteretic behavior of dilute polymer solutions in relaxation following extensional flow,'' J. Non-Newtonian Fluid Mech. **82**, 233–253 (1999).

Smith, D. E., and S. Chu, ''Response of flexible polymers to a sudden elongational flow,'' Science **281**, 1335–1340 (1998).

Solomon, M. J., and S. J. Muller, ''Flow past a sphere in polystyrene-based Boger fluids: The effect on the drag coefficient of finite extensibility, solvent quality and polymer molecular weight.,'' J. Non-Newtonian Fluid Mech. **62**, 81–94 (1996).

Sridhar, T., D. A. Nguyen, and G. G. Fuller, ''Birefringence and stress growth in uniaxial extension of polymer solutions,'' J. Non-Newtonian Fluid Mech. **90**, 299–315 (2000).

Stokes, Y. M., E. O. Tuck, and L. W. Schwartz, ''Extensional fall of a very viscous drop,'' Q. J. Mech. Appl. Math. **53**, 565–582 (2000).

Szabo, P., ''Transient filament stretching rheometry. I. Force balance analysis,'' Rheol. Acta **36**, 277–284 (1997).

Szabo, P., J. M. Rallison, and E. J. Hinch, ''Start-up of flow of a FENE-fluid through a 4:1:4 constriction in a tube,'' J. Non-Newtonian Fluid Mech. **72**, 73–86 (1997).

Talbott, W. H., ''Streaming birefringence in extensional flow of polymer solutions,'' PhD thesis, University of Michigan, Ann Arbor, MI, 1978.

Venerus, D. C., S. H. Zhu, and H.-C. Ottinger, ''Stress and birefringence measurements during the uniaxial elongation of polystyrene melts,'' J. Rheol. **43**, 795–813 (1999).

Wedgewood, L. E., D. N. Ostrov, and R. B. Bird, ''A finitely extensible bead-spring chain model for dilute polymer solutions,'' J. Non-Newtonian Fluid Mech. **40**, 119–139 (1991).